DETECTORS AS A FUNCTION OF LUMINOSITY AT e^+e^- MACHINES

G. Eigen

Dept. of Physics, University of Bergen, Allegaten 55, N-5007 Bergen, Norway
E-mail: eigen@asfys2.fi.uib.no

The performance of silicon-strip vertex detectors, drift chambers, CsI(Tl) electromagnetic calorimeters, and level-1 triggers used in present multipurpose detectors like BABAR is discussed in the context of operations in a high-luminosity environment.

1 Introduction

The successful start of the asymmetric B-factories last year has triggered discussions on physics accessible at luminosities of $\mathcal{L} = 10^{35} - 10^{36}\mathrm{cm}^{-2}\mathrm{s}^{-1}$.[1] Since such luminosities are technically feasible, questions have been raised, how subsystems of present multipurpose detectors like BABAR would perform in such a high-luminosity environment. This article presents a look at the impact of machine-related backgrounds on silicon-vertex detectors, drift chambers, CsI(Tl) electromagnetic calorimeters and level-1 (L1) trigger rates. Results are based on a BABAR study,[2] which was facilitated to cope with the planned PEP II luminosity upgrade relying on the experience with the response of BABAR to machine-related backgrounds in the first year of running. The data were parameterized in terms of first or second-order polynomials of beam currents and luminosity. For many measurements a linear dependence was already sufficient. In this article extrapolations are considered for three luminosity points: $\mathcal{L} = 0.65 \times 10^{34}$ cm^{-2}s^{-1}, 1.5×10^{34} cm^{-2}s^{-1}, and 5×10^{34} cm^{-2}s^{-1}. Expectations for the first two luminosity points are taken from the BABAR study,[2], while those for the third luminosity point represent my personal view. Without new data, I consider extrapolations to luminosities beyond $\mathcal{L} > 5 \times 10^{34}$ cm^{-2}s^{-1} unrealistic, because of large extrapolation uncertainties and additional backgrounds such as luminosity lifetime that become important at very high luminosities.[5] All extrapolations are based on the PEP II interaction region (IR) layout and bear a systematic error of at least a factor of two. It is not trivial to predict background levels in other IR layouts, such as that of KEK B.

The detector subsystems are subjected to different machine-related backgrounds. Electrons produce lost-particle backgrounds from beam-gas bremsstrahlung and Coulomb scattering in addition to synchrotron radiation. Positrons just produce lost-particle backgrounds from beam-gas bremsstrahlung. In addition, the interaction of the two beams yield further backgrounds. In the non-colliding mode a beam-gas cross term contributes, while in colliding mode further backgrounds originate from luminosity and beam-beam tails.

2 Silicon Vertex Detectors

Silicon vertex detectors, located closest to the beam, are exposed to high levels of radiation. The specific radiation dose depends both on beam currents and on the IR layout. For example, radiation levels at PEP II are expected to be higher than those at KEK B. In the BABAR detector the horizontal plane is most affected. While the low-energy ring (LER) produces high radiation levels in the forward-east region (FE-MID) of the detector, the high-energy ring (HER) affects the backward-west region (BW-MID). The dose rates in terms of beam currents (in units of [A]) are expected to be:

$$\begin{aligned} \mathrm{D_{SVT}}\ [\mathrm{kRad/y}] &= 128 \cdot \mathrm{I_{LER}} + 16 \cdot \mathrm{I^2_{LER}} \quad (\mathrm{FE-MID}), \\ \mathrm{D_{SVT}}\ [\mathrm{kRad/y}] &= 246 \cdot \mathrm{I_{HER}} + 9.1 \cdot \mathrm{I^2_{HER}} \quad (\mathrm{BW-MID}). \end{aligned} \tag{1}$$

For other regions the radiation dose is about a factor of ten smaller. Table 1 lists dose rates expected in the FE and BW regions of the horizontal plane for the three luminosity points. Figure 1 shows the total dose predictions for the BABAR silicon vertex tracker (SVT) in the high-radiation regions as a function of beam currents. Presently, the SVT is expected to survive a total dose of 2 MRad. Thus, with replacement of detectors in the horizontal plane the BABAR SVT should be operational at luminosities of $\mathcal{L} = 1.5 - 3 \times 10^{34}\mathrm{cm}^{-2}\mathrm{s}^{-1}$.

Radiation studies of microstrip detectors in the ATLAS semiconductor tracker (SCT) have demonstrated that silicon strip detectors can survive very high radiation levels in hadronic environments, if $\mathrm{p^+nn^+}$ detectors are used that are cooled. Before irradiation the depletion layer is formed between the $\mathrm{p^+ - n}$ junction. High-levels of ionization radiation effectively change the n-type silicon to p-type.[3,4] The depletion layer is shifted to the newly-formed $\mathrm{p - n^+}$ junction. Since for cost reasons detectors are readout on the $\mathrm{p^+}$ side, the shifting depletion layer causes a loss in signal. This design also introduces a substantial amount of material in front of subsequent detectors because of cooling and the need for twice as many layers as in a double-sided detector design, thus yielding increased multiple scattering. Though the ATLAS design is expected to work in high-luminosity e^+e^-

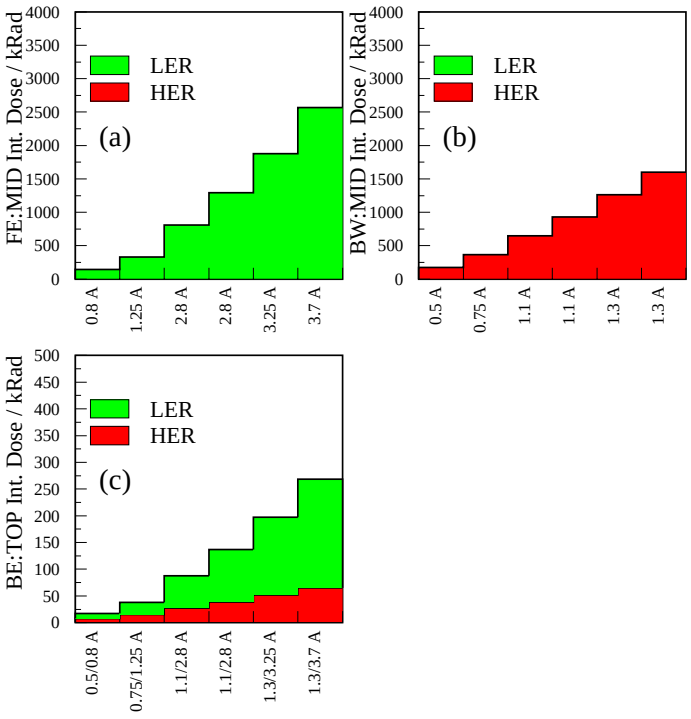

Figure 1: Integrated-dose predictions for the BABAR SVT in the horizontal plane versus peak beam currents, (a) for forward east region exposed to LER, (b) for backward west region exposed to HER, and (c) for top/bottom region exposed to both beams.

colliders, this needs to be checked in appropriate radiation studies.

3 Drift Chambers

The operation of drift chambers (DCH) is affected by machine backgrounds in three ways. First, the total current in the drift chamber drawn by the wires is dominated by the charge released by beam-related showers. This current is limited by the high-voltage system. Above this limit the chamber becomes non-operational. Though the limit can be increased by adding power supplies, high currents also contribute to the aging of the drift chamber. Permanent damage is expected to occur at charge-densities $Q_{max} > 0.1$ Cb/cm of wire. Second, the occupancy in the drift chamber due to backgrounds can hamper the reconstruction of physics events. Third, ionization radiation can permanently damage read-out electronics and digitizing electronics.

Drift chamber currents are of highest concern. Figure 2 shows the total drift chamber current as functions of LER and HER currents for a DCH high voltage of $U = 1900$ V. The data in the top left plot were fitted with a parabolic I_{LER} dependence using all points and both linear and parabolic I_{LER} dependences using points above 700 mA. For parameterizations in terms of I_{HER} (top-right plot) both linear and linear plus quadratic dependences for points above 150 mA were used. The best descriptions of the high-current regions are found for the linear plus quadratic parameterizations which discard low-current data. The effect of two beams in collision and out-of collision on I_{DCH} is shown in the bottom plots of Figure 2, confirming the presence of a beam-gas cross term and luminosity-related backgrounds. Including all effects the total DCH current is parameterized by:

$$\begin{aligned} I_{DCH}\ [\mu A] = 35.3 \cdot I_{LER} + 23.5 \cdot I_{LER}^2 + 77.2 \cdot I_{HER} \\ +46.3 \cdot I_{HER}^2 + 41.9 \cdot \mathcal{L} - 10, \end{aligned} \quad (2)$$

where beam currents and luminosity are given in units of [A] and $[10^{33}\mathrm{cm}^{-2}\mathrm{s}^{-1}]$, respectively. For $U = 1960$ V, drift chamber currents scale with a factor of 1.67. The drift chamber occupancy at 1900 V is parameterized by:

$$\begin{aligned} N_{DCH}\ [\%] = 0.044 + 0.191 \cdot I_{LER} + 0.0402 \cdot I_{LER}^2 \\ +1.03 \cdot I_{HER} + 0.113 \cdot I_{HER}^2 + 0.147 \cdot \mathcal{L}. \end{aligned} \quad (3)$$

Figure 3 shows the measured DCH occupancy in BABAR for high voltages of U = 1900 V and U = 1960 V. Due to the large spread of data points an extrapolation to high drift chamber currents bears large uncertainties.

Table 1 lists extrapolations of the total drift chamber current, occupancy and charge density on a wire for the three luminosity points. At $\mathcal{L} = 5 \times 10^{34}\mathrm{cm}^{-2}\mathrm{s}^{-1}$, I_{DCH} becomes large. For higher luminosities I_{DCH} basically just scales with $\mathcal{L}$. In addition, an effect from the luminosity lifetime is expected.[5] The total DCH current definitely exceeds the tolerable limit. Thus, a drift chamber will not be operational and one needs to explore other technologies. One possibility is the use solid state devices which could be integrated with the vertex detector. As mentioned before multiple scattering is an issue here. But since solid state devices have much better resolutions than drift chambers, a reduced number of layers with thin detectors may be acceptable. However, a detailed study needs to be devoted on this issue.

4 CsI(Tl) based Electromagnetic Calorimeters

For a thallium-doped CsI crystal calorimeter radiation damage and occupancy are the main issues. Figure 4 shows gain changes in crystals located in forward and backward regions of the BABAR electromagnetic calorimeter (EMC). Forward endcap crystals, located closest to the beams and thus affected most by radiation, show a gain loss of $\sim 6\%$ in the worst case. The corresponding light-yield reductions for the worst crystals in the forward barrel and backward barrel are $\sim 3.5\%$ and

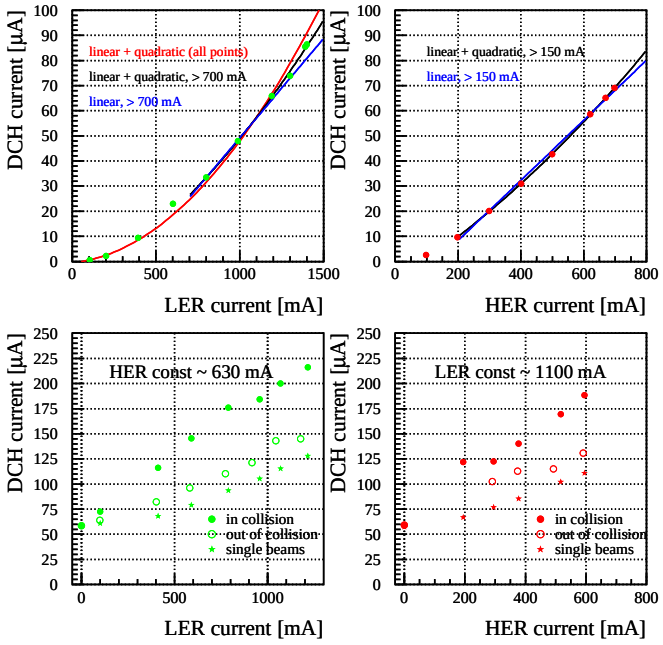

Figure 2: BABAR DCH currents versus beam currents, top plots for single-beam operation and bottom plots for two-beam operations. Solid points (open circles) in bottom plots show I_{DCH} for two beams in (out of) collision. The asterisk data points show the uncorrelated contributions from both beams.

$\sim$ 2%, respectively. These observations are consistent with the different background levels expected in these regions. Figure 5 shows BABAR data for the occupancy of crystals with energies above 1 MeV and for the number of crystals recording more than 10 MeV as a function of beam currents. Parameterizations in terms of beam currents ([A]) and luminosity ([10^{33}cm^{-2}s^{-1}]) yield:

$$\begin{aligned} O_{(E>1\ \mathrm{MeV})}\ [\%] &= 9.8 + 2.2 \cdot (I_{LER} + I_{HER}) + 1.4 \cdot \mathcal{L}, \\ N_{(E>10\ \mathrm{MeV})} &= 4.7 \cdot I_{HER} + 0.23 \cdot I_{HER}^2 + 2.4 \cdot I_{LER} \\ &\quad + 0.33 \cdot I_{LER}^2 + 0.6 \cdot \mathcal{L}. \end{aligned} \tag{4}$$

Note, that for $\mathcal{L} > 10^{34}$cm^{-2}s^{-1} the luminosity contribution is expected to be dominant. Extrapolations of $O_{(E>1\ \mathrm{MeV})}$ and $N_{(E>10\ \mathrm{MeV})}$ for the three luminosity points are presented in Table 1.

For luminosities of $\mathcal{L} < 1.5 \times 10^{34}$cm^{-2}s^{-1} the integrated radiation dose for CsI(Tl) crystals should be no problem, if observed light losses scale as expected. The impact of the large number of low-energy photons on the EMC energy resolution needs to be studied. It depends on the clustering algorithm and on digital filtering. Background rates can be reduced by improvements of the vacuum near the IR combined with effective collimation against e^+ from distant Coulomb scattering. For luminosities of $\mathcal{L} > 1 \times 10^{35}$cm^{-2}s^{-1}, however, light losses due to radiation damage become substantial and high occupancy levels severely hamper the performance. Therefore, present CsI(Tl) crystals are not suitable. Other scintillators, such as pure CsI crystals, need to be considered and an *R&D* program needs to be established.

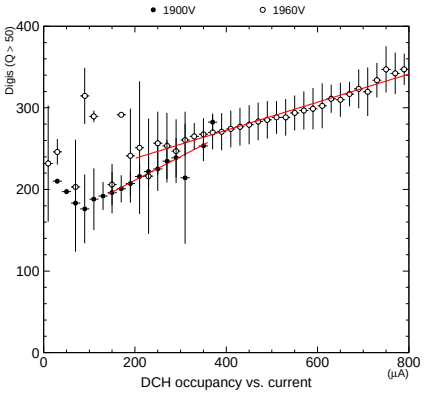

Figure 3: BABAR DCH occupancy as a function of I_{DCH} for U = 1900 V (solid points) and U = 1960 V (open points).

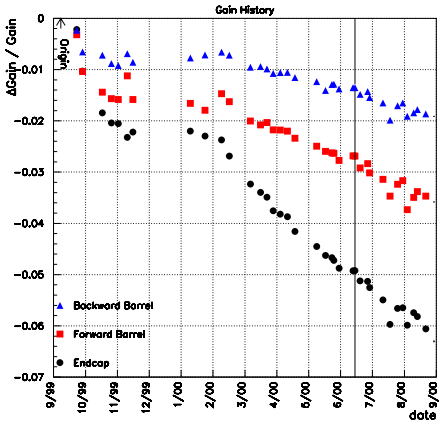

Figure 4: Gain changes of BABAR CsI(Tl) crystals in forward endcap, forward barrel and backward barrel versus time.

5 Level 1 Trigger

The level 1 trigger rate scales linearly both with beam currents and with luminosity:

$$\mathrm{L1\ [Hz]} = 130\ (\mathrm{cosmics}) + 130 \cdot I_{LER} + 360 \cdot I_{HER} + 70 \cdot \mathcal{L}. \tag{5}$$

Extrapolations for the three luminosity points are shown in Table 1. The L1 trigger rate measured in BABAR as a function of beam currents is plotted in Figure 6. The plot on the right shows a comparison of single beam operation (bottom), two-beam operation out of collision (middle)

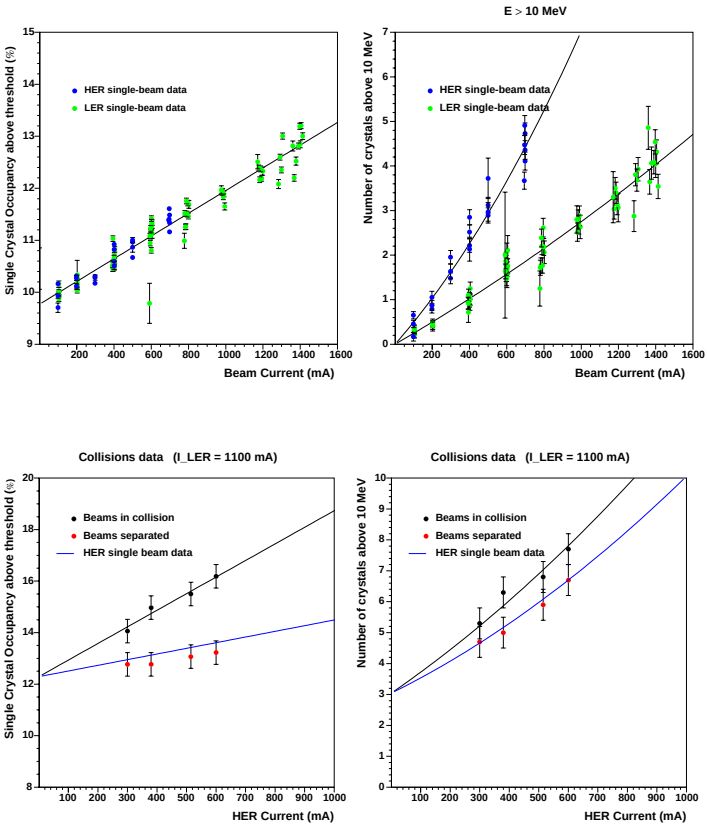

Figure 5: Average occupancy of BABAR EMC crystals above a 1 MeV energy readout threshold (left) and the number of crystals containing more than 10 MeV (right) versus beam currents. Top plots show single-beam data and bottom plots show the I_{HER} dependence for fixed $I_{LER} = 1100$ mA. The upper (lower) curves in bottom plots show fits for beams in (out of) collision.

and two-beam operation in collision (top). For luminosities above $1.5 \times 10^{34}\text{cm}^{-2}\text{s}^{-1}$ the BABAR trigger needs to be upgraded to cope with the increased trigger rates. The L1 trigger rate at very high luminosities could be reduced by implementing a rather stringent prescaling of Bhabhas, radiative Bhabhas and beam-gas backgrounds. This requires an appropriate tracking device used in the trigger. However, LHC experiments operating at a bunch crossing of 40 MHz are designed to accept an L1 trigger rate of 100 kHz.

6 Conclusions

For tracking and electromagnetic energy measurements other technologies need to be investigated. For silicon vertex detectors further radiation studies are needed. In order to have workable solutions for each subsystems ready, serious R&D has to start soon. A conventional muon system and a DIRC particle identification system with proper shielding are expected to work at luminosities above $1 \times 10^{35}\text{cm}^{-2}\text{s}^{-1}$.

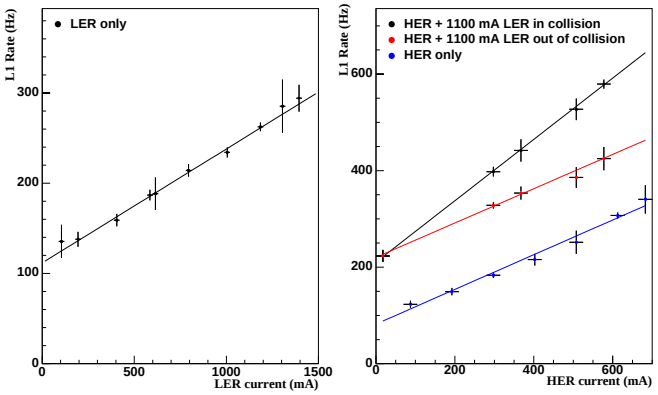

Figure 6: The L1 trigger rate versus I_{LER} (left) and I_{HER} (right).

Table 1: Extrapolations of dose rates in silicon vertex detectors, total current, occupancy, and charge density in drift chambers, occupancy of crystals with E > 1 MeV and number of crystals with E > 10 MeV in CsI(TL) calorimeters, and L1 trigger rate.

$\mathcal{L}_{peak}$ [$\text{cm}^{-2}\text{s}^{-1}$]	6.5×10^{33}	1.5×10^{34}	5.0×10^{34}
$\int \mathcal{L}dt$ [fb^{-1}]	55	400	2000
I_{LER}/I_{HER} [A]	2.8/1.1	3.7/1.3	4.6/1.5
D_{SVT} [kRad/y]	480/280	690/340	1300/930
I_{DCH} [μA]	680	1250	3000
N_{DCH} [%]	3.1	5	10
Q_{DCH} [mCb/cm]	15	50	> 100
$O_{(E>1\ MeV)}$ [%]	28	42	93
$N_{(E\ >\ 10\ MeV)}$	21	32	56
L1 [Hz]	1350	2130	4800

Acknowledgments

I would like to thank W. Kozanecki D. MacFarlane and B. Stugu for useful discussions. This work has been supported by the Research Council of Norway.

References

1. See *e.g.* articles by J. Alexander, K. Abe, Y. Kwon, S. Petrak, A. Falk, and J. Lee in these proceedings.
2. C. Hast *et al*, BaBar Note 522, 30 pp, (2000).
3. L. Andricek *et al*, Nuc.Ins.Meth. A409, 184 (1998).
4. G. Lutz, Semiconductor Radiation Detectors, Springer Verlag (1999).
5. M. Sullivan, talk at Beyond $10^{34}e^{+}e^{-}$ Workshop, Homestead, MI, June 16-18 (2000).